UCSF
UC San Francisco Previously Published Works

## Title

Integration of Genomic Sequencing Drives Therapeutic Targeting of PDGFRA in T-Cell Acute Lymphoblastic Leukemia/Lymphoblastic Lymphoma.

## Permalink

https://escholarship.org/uc/item/1wf5430g

## Journal

Clinical Cancer Research, 29(22)

## Authors

Ocasio-Martinez, Nicole
Tsai, Harrison
Li, Yuting
et al.

## Publication Date

2023-11-14

## DOI

10.1158/1078-0432.CCR-22-2562

Peer reviewed

eScholarship.org Powered by the California Digital Library
University of California

Author Manuscript

Author Manuscript

Author Manuscript

Author Manuscript

HHS Public Access

Author manuscript

*Clin Cancer Res*. Author manuscript; available in PMC 2024 May 14.

Published in final edited form as:

*Clin Cancer Res*. 2023 November 14; 29(22): 4613–4626. doi:10.1158/1078-0432.CCR-22-2562.

# Integration of genomic sequencing drives therapeutic targeting of PDGFRA in T-cell acute lymphoblastic leukemia/lymphoblastic lymphoma

**Jonathan Paolino**[*,1,2], **Boris Dimitrov**[*,1], **Beth Apsel Winger**[3,4], **Angelica Sandoval-Perez**[4], **Amith Vikram Rangarajan**[4], **Nicole Ocasio-Martinez**[1], **Harrison K. Tsai**[5], **Yuting Li**[1], **Amanda L. Robichaud**[1], **Delan Khalid**[1], **Charlie Hatton**[1], **Riaz Gillani**[1,2], **Petri Polonen**[6], **Anthony Dilig**[7], **Giacomo Gotti**[1,8], **Julia Kavanagh**[1], **Asmani A. Adhav**[1], **Sean Gow**[1], **Jonathan Tsai**[9], **Yen Der Li**[10], **Benjamin L. Ebert**[10], **Eliezer M. Van Allen**[10], **Jacob Bledsoe**[5], **Annette S. Kim**[9], **Sarah K. Tasian**[11], **Stacy L. Cooper**[12], **Todd M. Cooper**[13], **Nobuko Hijiya**[14], **Maria Luisa Sulis**[15], **Neerav N. Shukla**[15], **Jeffrey A. Magee**[16], **Charles G. Mullighan**[6], **Michael J. Burke**[17], **Marlise R. Luskin**[10], **Brenton G. Mar**[18], **Matthew P. Jacobson**[4], **Marian H. Harris**[5], **Kimberly Stegmaier**[1,2,19], **Andrew E. Place**[1,2], **Yana Pikman**[1,2]

[1.]Department of Pediatric Oncology, Dana-Farber Cancer Institute, Boston, MA

[2.]Division of Hematology/Oncology, Boston Children's Hospital, Boston, MA

[3.]Department of Pediatrics, Division of Hematology/Oncology, Benioff Children's Hospital and the Helen Diller Family Comprehensive Cancer Center, University of California San Francisco, San Francisco, CA

[4.]Department of Pharmaceutical Chemistry, University of California San Francisco, San Francisco, CA

[5.]Department of Pathology, Boston Children's Hospital, Boston, MA

[6.]Department of Pathology, St. Jude Children's Research Hospital, Memphis, TN

[7.]Integrated Oncology, Shelton, CT

[8.]Pediatrics, Fondazione IRCCS San Gerardo dei Tintori, Monza, Italy

[9.]Department of Pathology, Brigham and Women's Hospital, Boston, MA

[10.]Department of Medical Oncology, Dana-Farber Cancer Institute, Boston, MA

[11.]Division of Oncology and Center for Childhood Cancer Research, Children's Hospital of Philadelphia, Philadelphia, PA, and Department of Pediatrics and Abramson Cancer Center at the Perelman School of Medicine at the University of Pennsylvania, Philadelphia, PA

**Co-Corresponding Authors:** Dr. Andrew E. Place, Dana-Farber Cancer Institute, 450 Brookline Avenue, Boston, MA 02215, Andrew_place@dfci.harvard.edu, Phone: (617) 632-2313, Fax: (617) 632-5710; Dr. Yana Pikman, Dana-Farber Cancer Institute, 450 Brookline Avenue, Boston, MA 02215, Yana_pikman@dfci.harvard.edu, Phone: (617) 632-4754, Fax: (617) 632-4410.

*These authors contributed equally to this work

Conflicts of Interest:

YL is a current employee of Merck Pharmaceuticals. BGM is an employee of Blueprint Medicines. MPJ is a consultant to and shareholder of Schrodinger LLC, which licenses software used in this work. KS previously consulted for Kronos Bio, Astra-Zeneca, and Auron Therapeutics, receives grant funding from Novartis and Kronos Bio for an unrelated project and holds stock options with Auron Therapeutics.

Author Manuscript Author Manuscript Author Manuscript Author Manuscript

[12.]Department of Oncology, Johns Hopkins School of Medicine, Baltimore, MD

[13.]Seattle Children's Hospital, Cancer and Blood Disorders Center, Seattle, WA

[14.]Division of Pediatric Hematology/Oncology/Stem Cell Transplantation, Columbia University Irving Medical Center, New York, NY

[15.]Department of Pediatrics, Memorial Sloan Kettering Cancer Center, New York, NY

[16.]Division of Pediatric Hematology/Oncology, Washington University/St. Louis Children's Hospital, St. Louis, MO

[17.]Medical College of Wisconsin, Children's Hospital of Wisconsin, Milwaukee, WI

[18.]Blueprint Medicines, Cambridge, MA

[19.]Broad Institute of Massachusetts Institute of Technology and Harvard University, Cambridge, MA

## Abstract

**Purpose:** Patients with relapsed or refractory T-cell acute lymphoblastic leukemia (T-ALL) or lymphoblastic lymphoma (T-LBL) have limited therapeutic options. Clinical use of genomic profiling provides an opportunity to identify targetable alterations to inform therapy.

**Experimental Design:** We describe a cohort of 14 pediatric patients with relapsed or refractory T-ALL enrolled on the Leukemia Precision-based Therapy (LEAP) Consortium trial (NCT02670525) and a patient with T-LBL, discovering alterations in platelet-derived growth factor receptor-α (PDGFRA) in 3 of these patients. We identified a novel mutation in *PDGFRA*, p.D842N, and used an integrated structural modelling and molecular biology approach to characterize mutations at D842 to guide therapeutic targeting. We conducted a preclinical study of avapritinib in a mouse patient derived xenograft (PDX) model of *FIP1L1-PDGFRA* and *PDGFRA* p.D842N leukemia.

**Results:** Two patients with T-ALL in the LEAP cohort (14%) had targetable genomic alterations affecting *PDGFRA*, a FIP1-like 1 protein/PDGFRA (*FIP1L1-PDGFRA*) fusion and a novel mutation in *PDGFRA*, p.D842N. The D842N mutation resulted in PDGFRA activation and sensitivity to tested PDGFRA inhibitors. In a T-ALL PDX model, avapritinib treatment led to decreased leukemia burden, significantly prolonged survival, and even cured a subset of mice. Avapritinib treatment was well tolerated and yielded clinical benefit in a patient with refractory T-ALL.

**Conclusions:** Refractory T-ALL has not been fully characterized. Alterations in PDGFRA or other targetable kinases may inform therapy for patients with refractory T-ALL who otherwise have limited treatment options. Clinical genomic profiling, in real time, is needed for fully informed therapeutic decision making.

## Statement of Translational Relevance:

Patients with relapsed or refractory T-ALL/LBL have limited therapeutic options. We report the finding of activating *PDGFRA* alterations in two pediatric patients with highly treatment refractory T-ALL suggesting that recurrent *PDGFRA* alterations may be more common than previously appreciated in this high-risk subset. We used a structural modelling and molecular

Author Manuscript Author Manuscript Author Manuscript Author Manuscript

biology platform to characterize novel *PDGFRA* mutations. These studies expand the application of targeted drugs for patients with poor outcome T-ALL and demonstrate the potential benefit of treating patients with T-ALL/LBL and activating *PDGFRA* mutations with tyrosine kinase inhibitors. We report the first patient with T-ALL to have received avapritinib. This study will inform future therapies for patients with *PDGFRA* mutations.

**Keywords**

T-ALL; T-LBL; leukemia; lymphoma; PDGFRA; FIP1L1-PDGFRA; genomic sequencing; targeted therapy

## Introduction:

Integration of cancer genomic profiling has transformed clinical care for a number of cancers. In pediatrics, molecular profiling studies have enrolled patients with rare or difficult-to-treat cancers to define targetable alterations which can be matched with available therapies (1-8). These studies have demonstrated the ability of genomics to inform the use of targeted therapy, although few of the patients who received targeted therapies received them as part of clinical trials (1,8). Target-informed basket trials enable systematic study of targeted therapies. Eligible patients enroll in a screening study, allowing their tumor to be molecularly profiled and matched to an available therapeutic study. The National Cancer Institute (NCI) - Children's Oncology Group (COG) Pediatric Molecular Analysis for Therapy Choice (MATCH) study (NCT03155620), provides access to up to 13 potential treatment arms for patients with relapsed/refractory solid tumors or lymphomas with identifiable molecular targets (9). In a report of the first 1000 patients enrolled, 131 (46% of those identified with a targetable alteration matched to a study) enrolled on a therapeutic sub-study (9). The BEAT AML study (NCT03013998) for patients with acute myeloid leukemia (AML) ≥60 years of age demonstrated the feasibility of a 7-day precision medicine approach for therapy selection and highlighted the need to have numerous therapeutic sub-studies open simultaneously for various genomic alterations (10). Patients with genomically identified targets, but without an available clinical trial, may be able to receive approved therapy off-label, though investigational therapies may not be available or only available through compassionate use protocols from pharmaceutical companies. Systematic data collection and publication of rare, off-label use of targeted therapies are lacking and thus these experiences are unlikely to benefit treatment of future patients.

T-cell acute lymphoblastic leukemia (T-ALL) and T-cell lymphoblastic lymphoma (T-LBL) are aggressive lymphoid malignancies driven by an accumulation of genetic aberrations acquired during T-cell development (11,12). Several large studies have characterized the genomic landscape of newly diagnosed T-ALL (13,14), though relapsed/refractory T-ALL has not been comprehensively studied (15,16). Mutations resulting in dysregulated NOTCH1 signaling are present in over 70% of T-ALL and T-LBL and co-exist with numerous other genetic alterations involving cell cycle regulation, cell signaling, and epigenetic modulation (12,14). Understanding of T-ALL biology has led to the identification of several potential therapeutic targets, including lymphocyte cell-specific protein-tyrosine kinase

Author Manuscript Author Manuscript Author Manuscript Author Manuscript

(LCK), JAK/STAT or PI3K/AKT pathways, or CDK4/6 (17,18). While considerable success has been achieved using immunotherapy for patients with B-cell ALL (B-ALL), effective immunotherapeutic approaches for T-ALL are lacking (19). Thus, despite the pre-clinical development of several potentially promising therapeutic strategies, effective treatment options for patients with relapsed/refractory T-ALL/LBL remain limited, and outcomes are dismal for these patients (20).

Class III receptor tyrosine kinases (RTKs) are a family of homologous, transmembrane signaling proteins responsible for initiating and amplifying signals for cell proliferation and survival (21,22). Activating mutations in RTK platelet derived growth factor receptor-α (*PDGFRA*) include missense mutations in the activation loop (A-loop) and gene fusions, such as the FIP1-like 1 protein/*PDGFRA (FIP1L1-PDGFRA)* fusion (21-23). A-loop missense mutations can disrupt key interactions of the A-loop, favoring the active conformation of the protein and resulting in constitutive activation (22). These mutations are central to the pathogenesis of gastrointestinal stromal tumors (GIST) and may be inhibited using ATP-competitive tyrosine kinase inhibitors (TKIs), such as imatinib (21,24). TKI resistance mutations, particularly *PDGFRA* p.D842V in exon 18, can be present at initial diagnosis or arise during TKI therapy (24-26). Avapritinib (BLU-285) is a potent and highly selective TKI targeting PDGFRA and KIT (27). It was recently approved for the treatment of adults with unresectable or metastatic GIST harboring *PDGFRA* exon 18 mutations, including *PDGFRA* p.D842V, as well as patients with advanced systemic mastocytosis and related disorders (28,29). In contrast to GIST, *PDGFRA* missense mutations are rare in acute leukemia (26,30). To date, five patients with AML have been reported to have received avapritinib (31,32).

Fusions involving *PDGFRA* can also lead to kinase activation. A cytogenetically cryptic deletion on chromosome 4q12 leads to the *FIP1L1-PDGFRA* fusion (33). The resultant protein disrupts the inhibitory interactions of the kinase with the juxtamembrane domain and results in constitutive kinase activity. The *FIP1L1-PDGFRA* fusion is found in idiopathic hypereosinophilic syndrome (HES), chronic eosinophilic leukemia (CEL), and AML, and can be inhibited with imatinib or dasatinib (23,34,35). The use of TKIs has transformed therapy for patients with hematological malignancy with a *FIP1L1-PDGFRA* fusion and re-defined these diseases as myeloid/lymphoid neoplasms with eosinophilia and tyrosine kinase gene fusions by the World Health Organization (36).

We report a series of 14 patients with relapsed or refractory T-ALL enrolled on the Leukemia Precision-based Therapy Consortium (LEAP) trial (NCT02670525). Two patients with refractory T-ALL (2/14, 14%) had genomic alterations involving *PDGFRA*. Additionally, we report a young adult patient with T-LBL with a *PDGFRA* translocation. We used an integrated structural and molecular biology approach to study mutations at the D842 residue to further inform potential targeted therapies for patients. This report highlights the importance of clinical genomics to promptly identify targetable alterations for patients with high-risk leukemia and to integrate targeted therapies into clinical care, as well as the need for effective pipelines for novel variant validation.

Author Manuscript Author Manuscript Author Manuscript Author Manuscript

## Methods

### Patient Information and leukemia profiling

Patients listed in Table 1 were enrolled on the Leukemia Precision-based Therapy (LEAP) Consortium trial (NCT02670525). Representativeness of this cohort is described in Supplementary Table 1. The institutional review board of each participating institution approved the protocol before enrolling patients. Written informed consent was obtained from patients and/or parents/guardians before study enrollment and initiation of therapy. At the time of enrollment, patients had a leukemia sample or DNA derived from a leukemia sample sent for sequencing using a CLIA certified next-generation sequencing (NGS) panel profiling 95 genes commonly mutated in leukemia (Rapid Heme Panel) (37). For the LEAP study T-ALL cohort, a subset of the patients had fusion testing using AMPSeq fusion panel or RNASeq. Clinical data, cytogenetics, fluorescence *in situ* hybridization (FISH), and sequencing results were reviewed by an expert panel of physicians. Gene fusions were assessed using an ArcherDX FusionPlex® Heme (v.2) panel of 72 target genes. Patient A1 had a tumor sample profiled using Oncopanel assay (38). Seven patients in this cohort were described previously (1). T-ALL sequencing data and analysis was previously reported and deposited as described (13).

Avapritinib was provided as part of a single patient IND (BLU-285-19-310 / IND 144524). Chart reviews were performed for the patients with *PDGFRA* alterations. and relevant data extracted under a Dana-Farber Cancer Institute Institutional Review Board (IRB) approved protocol.

### Vectors and constructs

pHAGE-PDGFRA (RRID: Addgene_116769, generous gift of Gordon Mills & Kenneth Scott) was used to generate *PDGFRA* p.D842N, p.D842V, p.D842H, p.D842E, p.D842Q, p.D842T, p.D842H/p.H845D, and p.R383C. Mutations were generated using QuickChange II XL Site-Directed Mutagenesis Kit (Agilent Cat. No. 200521) following the manufacturer's instructions. Mutagenesis primers are listed in Supplementary Table 2. All mutations were confirmed by Sanger sequencing.

### Cell culture and viability assays

Ba/F3 cells were purchased from DSMZ (Cat. No. ACC-300, RRID: CVCL_0161) and identity validated by DSMZ. Untransformed cells maintained IL-3 dependence for growth during experiments. Mycoplasma testing was done using Lookout Mycoplasma PCR Detection kit (Sigma-Aldrich). Cells were maintained in RPMI-1640 (Cellgro) supplemented with 1% penicillin/streptomycin (PS), 10% FBS (Sigma-Aldrich) and murine IL-3 (PeproTech) at 37°C with 5% $C0_2$. For IL-3 independence assays, following transduction with either *PDGFRA, PDGFRA* p.D842N, p.D842H, p.D842E, p.D842Q, p.D842T, p.D842H/p.H845D, or p.R383C, Ba/F3 cells were selected with puromycin and were cultured without IL-3. Viability was assessed for each cell line when grown without IL-3.

Author Manuscript Author Manuscript Author Manuscript Author Manuscript

### Lentiviral generation and infection

HEK293T cells (RRID: CVCL_0063) were transfected with 8 μg of *PDGFRA* vector, 2 μg of pCMV-VSV-G, and 4 μg of *PAX*2 vectors using the X-tremeGENE 9 HP system (Sigma Aldrich Cat. No. 6366236001). The resulting viral supernatants were harvested after 72 hours. Four million Ba/F3 cells were infected for 3 hours at 37°C with lentiviral supernatant and polybrene (Santa Cruz Biotechnology Cat. No. SC-134220). Cells were selected 48 hours later with 1 μg/ml puromycin (Invitrogen Cat No. ant-pr-1) for three days.

### Drug sensitivity testing

Imatinib (Cat. No. S1026), dasatinib (Cat. No. S1021), ponatinib (Cat. No. S1490), and avapritinib (Cat. No. 8553) were purchased from Selleck Chemicals, LLC.

IL-3 independent Ba/F3 cells expressing *PDGFRA* p.D842N, p.D842H, and p.D842H/p.H845D were treated with increasing doses of imatinib, dasatinib, ponatinib or avapritinib for three days. For control, *PDGFRA* wild-type Ba/F3 cells were grown in the presence of IL-3 and tested for drug sensitivity. Viability was evaluated using the CellTiter-Glo Luminescent Cell Viability Assay (Promega), measured using FLUOstar Omega from BMG Labtech. The $IC_{50}$ values were determined using GraphPad Prism version 9 software (RRID: SCR_002798).

### Immunoblotting

Cells were lysed in Cell Signaling Lysis Buffer (Cell Signaling Technology Cat. No. 9803S) and resolved by gel electrophoresis using Novex 4-12% Bis-Tris Gels (Life Technologies Cat. No. NP0322BOX), transferred to a PVDF membrane (Life Technologies Cat. No. 88518) and blocked 1 hour in 5% BSA (Sigma Cat. No. A7906). Blots were incubated in primary antibody to p-PDGFRA-Tyr754 (Cell Signaling Technology Cat. No. 9360, RRID: AB_10691547), PDGFRA (Cell Signaling Technology Cat. No. 9360, RRID: AB_10691547), pSTAT5- Tyr694 (Cell Signaling Technology Cat. No. 9351, RRID: AB_2315225), and STAT5 (Cell Signaling Technology Cat. No. 25656, RRID: AB_2798908), followed by exposure to anti-rabbit HRP secondary antibodies (Cell Signaling Technology Cat. No. 7074, RRID: AB_2099233). Detection of bound antibody was performed using SuperSignal West Dura (Thermo Scientific Cat. No. 37071).

### Equilibrium Molecular Dynamics Simulations

The starting conformation of the auto-inhibited inactive state of the PDGFR kinase was taken from the protein data bank (PDB ID: 5k5x) (39). The single mutations D842V, D842N, D842H, H845D, and the double mutation D842H/H845D were introduced. For the particular case of the double mutation, two protonation states of the histidine were considered: neutral (epsilon protonated, HIE) and fully protonated (HIP). Additionally, the unfolded tripeptides GXG (X=D, V, N, and H) were obtained from the *pmx* server (40).

The following combination of force fields was used: Amber14SB (41) for the protein, Joung ions parameters for the ions (42), and the TIP3P model (43) for the water molecules. All simulations were performed at constant pressure and temperature. The pressure was kept constant at 1 bar with a coupling constant of 1 ps using the Berendsen barostat.

Author Manuscript Author Manuscript Author Manuscript Author Manuscript

The temperature was kept at 310 K with a time constant of 0.5 ps, using the Nose-Hoover thermostat coupled individually to the protein and solvent. Long-range electrostatic interactions were treated with the particle mesh Ewald (PME) algorithm (44). Short-range interactions modeled with the Lennard-Jones potential were subjected to a cut-off distance of 1 nm. LINCS (45) constraints were applied to hydrogens and SETTLE (46) constraints to the angles and bonds of the water molecules.

All equilibrium simulations were performed using the package GROMACS, version 2020.1 (RRID: SCR_014565). The potential energy of the protein was minimized for 50000 steps in vacuum. Then, ~17340 water molecules, NaCl ions at concentration 0.15 M, and additional counter ions to neutralize the system, were added. The solvated system was minimized for 50000 steps, applying the steepest descent algorithm. Three replicas were generated from these minimized systems. The solvent was equilibrated in each replica for ten ns with the protein positioned-restrained on the heavy atoms. The positional restraints were removed and production runs of 500 ns per replica were performed for a total simulation time of 9 μs.

## Free Energy Calculations

Alchemical free energy calculations were used to compute the effect of mutation on the thermodynamic stability of the PDGFRA kinase domain in its inactive state in reference to the wild-type protein. The thermodynamic cycle for single mutations is presented in Supplementary Figure 1A and the thermodynamic cycle for the double mutation is presented in Supplementary Figure 1B. The double mutations were assumed to be a symmetrical exchange between aspartic acid and histidine, i.e., D842H and H845D, which implies that in the unfolded state, such double mutation ($\Delta G1+\Delta G5$) should result in contribution of $\Delta G\approx 0$.

Using the alchemical transformation from wildtype ($\lambda 0$) to mutant ($\lambda 1$), we were able to calculate the work needed to transform the system from one state to another through a nonphysical pathway . The Bennett acceptance ratio (BAR) as a maximum likelihood estimator, proposed by *Shirts et al.* (47), was used to derive the equilibrium free energy ($\Delta G$) from the work distribution associated to “forward” ($P_fW$) and “reverse” ($P_rW$) transitions. Finally, the $\Delta G$ uncertainty was calculated by bootstrapping, solving the last equation 100 times from randomly selected forward and reverse data sets.

We extracted 600 conformations of the inactive PDGFRA kinase from the MD-equilibrium simulations, which served as starting structures for the alchemical transformation. The hybrid topology was obtained using the pmx tool (40). All the starting simulations were minimized for 100000 steps and further equilibrated for 500 ps with position restraints in the protein, previous to performing forward or backward transformations of 100 ps each. A total of 450 starting conformations were extracted from the MD-equilibrium simulations of the GXG (X=H, V, D, N) peptides and used as starting structures of the forward and backward calculations, following the previously described protocol. All simulations corresponding to the alchemical transformations were done using GROMACS version 4.6 with an integrated soft core potential function, using the previously described parameters. The final free energies and their associated uncertainty were estimated using the BAR method implemented in the *pmx* set of tools.

Author Manuscript Author Manuscript Author Manuscript Author Manuscript

### *In vivo* study

Primary ALL cells were obtained from a pediatric patient with relapsed T-ALL at Boston Children's Hospital/Dana-Farber Cancer Institute on an approved institutional research protocol (NCT02670525). Informed consent was obtained prior to sample acquisition in accordance with the Declaration of Helsinki. Animal studies were conducted under an Institutional Animal Use and Care Committee (IACUC)-approved protocol in accordance with the Panel on Euthanasia of the American Veterinary Medical Association's guidelines. Patient leukemia cells were injected by tail vein into NSG mice to establish the primary PDX model. Subsequently, $1x10^6$ cells from primary PDX spleens were injected into secondary 8-week-old female NSG mice for the experimental study. After flow cytometric confirmation of ≥1% CD45+ human ALL (Invitrogen Cat No. 17-9459-42) in murine peripheral blood, mice were randomized to treatment with vehicle or avapritinib 30 mg/kg per os (PO) daily for 28 days. Planned disease evaluations were conducted at days 7 and 28 of treatment. These evaluations included spleen weight and evaluation of human CD45 positive (hCD45+) leukemic blasts in the peripheral blood, bone marrow, and spleen as measured by flow cytometry. Mice in the treatment group that developed recurrent disease following discontinuation at 28 days were re-treated for a second 28-day course. Leukemia cells obtained from the PDX model were profiled using OncoPanel (38).

### Data Availability

T-ALL sequencing data was previously reported and deposited as described (13,14). TARGET ALL data may be accessed through the TARGET website at https://ocg.cancer.gov/programs/target/data-matrix. The remaining non-TARGET data is accessible through St. Jude Cloud at https://platform.stjude.cloud/data/cohorts?dataset_accession=SJC-DS-1009 (13). Data from patients on the LEAP trial is included within this manuscript and partly published previously (1). Corresponding authors are available to provide any additional data.

## Results

### Identification of *PDGFRA* alterations in three patients with T-ALL/T-LBL

Between July 2016 and May 2022, 338 patients with relapsed/refractory or high-risk leukemia or myelodysplastic syndrome (MDS) were enrolled on the LEAP Consortium trial (NCT02670525) across 15 pediatric cancer hospitals (1). A diagnostic bone marrow or peripheral blood sample was submitted for sequencing at the time of enrollment. Samples were sequenced using a CLIA-certified DNA based NGS panel profiling 95 genes commonly mutated in leukemia (Rapid Heme Panel) (1). A sub-group of patients had fusion testing using multiplex RT-PCR, AMPSeq fusion panel, or RNASeq (48). Clinical data, cytogenetics, FISH, and sequencing results were reviewed by an expert panel of physicians.

The LEAP study enrolled 14 patients with relapsed or refractory T-ALL (Table 1, seven patients previously described (1)). Mutations in RAS, JAK/STAT, and PI3K/PTEN signaling pathways have previously been reported in association with relapsed/refractory T-ALL (15,30). In our cohort 9 patients (9/14, 64%) had mutations in genes involved in these signaling pathways. *STIL-TAL1* fusions, also previously reported as associated with

Author Manuscript Author Manuscript Author Manuscript Author Manuscript

relapsed T-ALL (49), were present in 3 patients (3/14, 21%). Interestingly, two patients with primary refractory T-ALL had *FIP1L1-PDGFRA* fusions (Table 1). Patient 146 in this cohort also had a novel *PDGFRA* mutation, p.D842N.

Patient 146 was a 16-year-old female with T-ALL with peripheral blood flow cytometry showing 90% abnormal T lymphoblasts and blasts in her central nervous system (CNS) at the time of diagnosis (Supplementary Table 3). Her leukemia was refractory to initial therapy and she received multiple salvage regimens (50,51) (Supplementary Table 4). She was enrolled on the LEAP study with 1% disease in the bone marrow. Following a brief complete remission, she was found to have a combined CNS and bone marrow relapse. She received multiple relapse regimens (Supplementary Table 4) but evaluation on Day 44 post immuno-therapy again demonstrated leukemia (Figures 1A and 1B). Repeat Rapid Heme Panel revealed a novel mutation that was characterized as a variant of unknown significance, *PDGFRA* p.D842N. Read counts suggested copy number loss of a 5' segment of *PDGFRA*, pointing to a possible fusion involving *PDGFRA* (Figure 1C). Targeted fusion testing using an AMPSeq panel showed *STIL-TAL1* and *FIP1L1-PDGFRA* fusions (Supplementary Table 3).

Patient 230 was a 6-year-old male with T-ALL who did not respond to induction chemotherapy per COG AALL1231 (52) (Supplementary Table 3). He started chemotherapy as per COG AALL0434 but died due to multi organ failure (50). Molecular profiling identified *STIL-TAL1* and *FIP1L1-PDGFRA* gene fusions.

We compared *PDGFRA* expression from samples from patients 146 and 230 with expression in a chronic eosinophilic leukemia cell line, EOL1, which is characterized by *FIP1L1-PDGFRA* fusion. Both samples had *PDGFRA* expression in the range that was seen in EOL1 (Figure 1D). For patient 230, *PDGFRA* expression was much higher at the time of refractory disease compared to a sample obtained from diagnosis (Figure 1D). *PDGFRA* expression for these samples was higher than all other clinical T-ALL samples profiled using the Boston Children's Hospital Heme Malignancy AMPSeq Fusion Panel from July 2020 to November 2021, raising the possibility of using this expression analysis for identification of targetable alterations in the absence of fusions in patients.

Following identification of *FIP1L1-PDGFRA* fusions in our LEAP trial cohort, we identified another patient with T-LBL with this same fusion. Patient A1, is a 27-year-old male who presented with several months of progressive neck pain and was found to have a large mediastinal mass with core biopsy demonstrating the presence of T-LBL. Treatment was initiated with R-EPOCH (rituximab, etoposide, prednisone, vincristine, cyclophosphamide, doxorubicin), and later transitioned to a pediatric-inspired ALL regimen, Cancer and Leukemia Group B (CALGB) 10403 (53-55). Oncopanel testing revealed a *FIP1L1-PDGFRA* fusion and other variants of unknown significance, including a *PDGFRA* p.R383C mutation (Supplementary Table 3) (38).

To determine the prevalence of PDGFRA alterations in T-ALL, we analyzed T-ALL genomic data reported in Brady et al. (13), a combination of samples from 264 children and young adult patients enrolled on COG AALL0434 and for whom tumor and remission

Author Manuscript Author Manuscript Author Manuscript Author Manuscript

samples were available (TARGET project (14)), as well as 202 additional T-ALL samples, for the presence of *PDGFRA* alterations. We identified 1 sample (PATBGC) with relatively high expression of *PDGFRA* based on RNASeq and with a tumor karyotype of 46,XX,t(4;12;9)(q13;p13q34)[20], consistent with a complex translocation involving *PDGFRA*, which is located at 4q12. Whole genome sequencing showed a three-way complex rearrangement, with a breakpoint in chromosome 4, 146,745 base pairs upstream of the *PDGFRA* gene, resulting in a *ETV6-PDGFRA* translocation.

## Molecular dynamics predicts that D842 interacts with several residues to hold the kinase in an inactive conformation

Interpretation of clinical sequencing is often complicated by the presence of variants of unknown significance. For a mutation within a protein with a known inhibitor, validation of novel alterations is particularly important as it may inform therapy selection. For patient 146, the presence of the novel *PDGFRA* p.D842N mutation suggested the possibility of TKI resistance, given the well described imatinib resistance mutation, *PDGFRA* p.D842V (24,25). We thus used a multi-faceted approach to study the *PDGFRA* p.D842N variant.

We first used molecular dynamics to predict the impact of the *PDGFRA* p.D842N mutation on kinase activation. The published crystal structure of the inactive kinase domain of *PDGFRA* shows a typical type 3 receptor tyrosine kinase fold with an autoinhibitory JM domain (orange), the activation loop collapsed in on the active site (pink), and the phosphate-binding loop (P-loop, green) positioned to orient ATP for catalysis (Figure 2A) (39). Residue D842 is located on the activation loop (Figure 2B). Our initial hypothesis was that the interaction between the negatively charged side chain of D842 and the positively charged H845 forms a salt bridge that plays a critical role in holding the activation loop in the inactive conformation; however, molecular dynamics simulations on wild-type PDGFRA did not support this hypothesis. The side chain of D842 establishes hydrogen bonds with 1) the backbone amide groups of M844 in the activation loop and A603 and S601 in the P-loop, and, 2) the side chains of R554 and Y555 in the JM domain, holding the kinase in the inactive conformation (Supplementary Figure 1A-B and Supplementary Table 5).

## Alchemical free energy calculations predict that activating mutations destabilize the autoinhibited state

*In vitro* biochemistry and cell biology have been critical to understanding the significance of previously uncharacterized variants in kinases and other oncogenic proteins. However, these experiments can rarely be completed on a timeline required to inform clinical care. We hypothesized that alchemical free energy calculations could be used as a computational method to predict the activity of uncharacterized kinase variants.

We used alchemical free energy calculations to estimate the overall effect of a mutation on the thermodynamic stability of the PDGFRA kinase. Following the thermodynamic cycle (Figure 2C), we calculated the ΔΔG value, which quantifies the effect of introducing a mutation in the PDGFRA kinase compared to the wildtype protein; a negative ΔΔG indicates that the inactive, auto-inhibited PDGFRA kinase is destabilized, and has a higher probability of being activated by the mutation. The free energy calculations predict that the D842V

Author Manuscript Author Manuscript Author Manuscript Author Manuscript

mutation is the most activating, whereas the H845D mutation is the least activating (Figure 2D and Supplementary Figure 1A-B).

To test the predictions from the molecular dynamics and alchemical free energy calculations, we expressed mutant *PDGFRA* genes in Ba/F3 cells. Expression of *PDGFRA* p.D842V, *PDGFRA* p.D842N, and *PDGFRA* p.D842H in Ba/F3 cells led to IL-3 independent growth (Figure 3A), confirming the activating nature of these mutations. Expression of *PDGFRA* p.H845D did not lead to IL-3 independent growth, consistent with the free energy calculations that showed H845D was the least activating mutation, while D842V was the most activating. We also made the double mutant *PDGFRA* p.D842H/p.H845D to biochemically test the hypothesis that the electrostatic interactions between these residues were critical to holding the kinase in the active position. We hypothesized that with the charge swap (*PDGFRA* p.D842H/p.H845D), the kinase would remain in the inactive conformation because the electrostatic interaction would still be present. However, consistent with the molecular dynamics and free energy results, the charge swap did not hold the kinase in the inactive conformation, as evidenced by IL-3 independent growth in the *PDGFRA* p.D842H/p.H845D Ba/F3 cells.

We then tested the effect of three other mutations at the D842 amino acid. Interestingly, expression of *PDGFRA* p.D842Q (selected because of its similarity to D842N), *PDGFRA* p.D842T (selected because it is isosteric to the D842V mutation), and *PDGFRA* p.D842E (selected because it conserves the charge of the endogenous amino acid and is the most conservative mutation) all led to IL-3 independent growth, informing the critical role for D842 in maintaining the inactive *PDGFRA* conformation (Figure 3B).

Patient A1 was also found to have a *PDGFRA* variant of unknown significance, p. R383C. This mutation is located within exon 8 of *PDGFRA* and is part of the extracellular domain (56). Expression of *PDGFRA* p.R383C in Ba/F3 cells did not lead to IL-3 independent growth (Supplementary Figure 2A), highlighting the need to validate variants of unknown significance to inform pathogenesis and possible therapy.

### *PDGFRA* p.D842N is sensitive to tyrosine kinase inhibition

Mutations in *PDGFRA* in GIST result in sensitivity to tyrosine kinase inhibition with imatinib, which is used routinely for therapy. *PDGFRA* p.D842V is a well-described mutation leading to resistance to imatinib in patients with GIST (24). This mutation has been reported at the time of initial diagnosis as well as arising during TKI therapy (25). Given the uncertain consequences of *PDGFRA* p.D842N, we tested Ba/F3 cells expressing *PDGFRA* mutations for sensitivity to imatinib, dasatinib, ponatinib, or avapritinib. Expression of *PDGFRA* p.D842V, p.D842N, p.D842H, and double mutated p.D842H/p.H845D in Ba/F3 cells all led to an increase in the basal level of phosphorylated PDGFRA (pPDGFRA). Cells expressing *PDGFRA* p.D842V were resistant to imatinib and less sensitive to dasatinib and ponatinib than other mutant cell lines tested (Figure 3C and 3D, Supplementary Figure 2B-C). All tested mutations resulted in sensitivity to avapritinib, including a decrease in pPDGFRA and pSTAT5 across all tested cell lines with avapritinib treatment (Figure 3E).

Author Manuscript Author Manuscript Author Manuscript Author Manuscript

### Development of a patient-derived xenograft model and response to avapritinib

To study the combination of *FIP1L1-PDGFRA* and *PDGFRA* p.D842N *in vivo*, we developed a patient-derived xenograft (PDX) model from leukemia cells obtained from Patient 146. Mononuclear cells isolated from a peripheral blood sample were injected into an NSG mouse with rapid leukemia engraftment. Bone marrow and spleen were replaced with leukemia cells in the NSG mouse (Figure 4A and 4B), with flow cytometry from cells extracted from the mouse confirming a similar immunophenotype to that of the patient (Figure 4C). We confirmed the presence of the *FIP1L1-PDGFRA* fusion using the NGS fusion assay as well as FISH (Figure 4D, 4E, Supplementary Table 6). RNASeq performed on spleen cells derived from the PDX model demonstrated the presence of the *PDGFRA* p.D842N mutation within the fusion reads (Figure 4F). Interestingly, three fusion calling algorithms, STAR-Fusion, ChimPipe, and FusionCatcher, did not detect the fusion transcript within RNASeq data, although it was identifiable by manual review and confirmed with FISH and a targeted fusion panel (57-59). This highlights a possible benefit of a clinically validated targeted panel over unbiased RNASeq for clinical purposes.

We then used the established PDX model to conduct a preclinical study of avapritinib. NSG mice were injected with cells from this PDX, and after disease was established, mice were randomized to receive vehicle or avapritinib. After seven days of treatment, avapritinib treated mice had a decrease in spleen size and leukemia burden in the bone marrow and spleen (Figures 5A and 5B). Bone marrow evaluation after seven days of avapritinib treatment showed a decrease in pSTAT5, showing on-target activity of avapritinib (Figure 5C).

The avapritinib treatment was continued for 28 days. After 28 days of treatment, there was an even greater effect of avapritinib, with a marked difference in spleen size and leukemia burden in peripheral blood, bone marrow, and spleen in mice treated with avapritinib (Figure 5D and 5E). There was a significant difference in peripheral blood leukemia burden in mice treated with avapritinib versus control, as measured by hCD45 (Figure 5F). Avapritinib therapy resulted in a significant survival benefit (Figure 5G). Two mice in the treatment group demonstrated durable remission following discontinuation of avapritinib with no evidence of disease recurrence (Figure 5H). Of these, one mouse died following 352 days of remission and had no evidence of leukemia at the time of death. The other remains alive at >400 days of remission.

Three of the five mice in the treatment cohort developed recurrent leukemia following discontinuation of avapritinib. Treatment was re-initiated in these three mice with a significant decrease in leukemia burden in the bone marrow, suggesting no overt resistance to avapritinib and the need for prolonged therapy with a TKI in *PDGFRA* mutant acute leukemia (Figure 5H and Supplementary Figure 2D). In patients, treatment with a combination of avapritinib with chemotherapy or other targeted agents may be needed for cure.

Author Manuscript Author Manuscript Author Manuscript Author Manuscript

### Clinical use of PDGFRA-targeted therapy for T-ALL and T-LBL

For patient 146, the discovery of the *PDGFRA* p.D842N and *FIP1L1-PDGFRA* led to the initiation of dasatinib in combination with dexamethasone and vincristine. Despite this, her peripheral blast count continued to rise over a period of 2 weeks (Figure 5I). A single patient Investigational New Drug (IND) application was filed for use of avapritinib. Given the rapid leukemia progression, she received a single dose of cyclophosphamide and etoposide before avapritinib became available. She was started on avapritinib 100 mg daily with a dramatic response in peripheral blood blast count (Figure 5I). She continued daily avapritinib with maintained response in the peripheral blood blast count and improvement in leukemia-related neuropathic pain.

Avapritinib was overall well tolerated by our patient. She experienced grade 3 tumor lysis syndrome which began concurrently with the start of avapritinib and continued through day 3 of treatment. This was assessed as possibly being related to avapritinib. Other recorded adverse events were fever and neutropenia, bacteremia, hypoxemia, and myelosuppression. All were grade 3 and assessed as unrelated to avapritinib. Bone marrow evaluation after two cycles of avapritinib (total of 48 days of treatment) revealed a hypocellular marrow with 20-30% involvement by residual leukemia, down from 85% at the start of avapritinib. A third cycle of avapritinib in combination with cyclophosphamide and etoposide was planned; however, the patient and family elected to stop cancer-directed therapy. The patient died from disease progression 30 days after stopping avapritinib.

For Patient A1, the discovery of *FIP1L1-PDGFRA* fusion at the time of initial diagnosis led to the addition of imatinib 100 mg daily to the CALGB 10403 chemotherapy regimen. The patient received daily imatinib monotherapy following completion of chemotherapy and remained in remission for 40 months before having disease recurrence. The *FIP1L1-PDGFRA* fusion and *PDGFRA* p.R383C VUS were not detected at the time of relapse.

## Discussion

In 2001, imatinib was the first tyrosine kinase inhibitor approved by the Food and Drug Administration (FDA), heralding the era of precision medicine for cancer therapy and transforming the treatment of chronic myelogenous leukemia characterized by the now targetable *BCR-ABL1* fusion. Since that time, dozens of kinase inhibitors have been developed with increased potency and selectivity against a variety of pathogenic kinases. Availability of targeted inhibitors makes genomic profiling of cancer imperative, with the possibility of integrating targeted therapy for genomically defined tumors. The use of imatinib and other TKIs has transformed the treatment of ALL with *BCR-ABL1* fusions and has also been used for other fusion targeting in B-ALL (60,61).

Discovery of the *FIP1L1-PDGFRA* fusion in HES allowed for therapeutic targeting of PDGFRA and substantially improved outcomes for this disease (23). In our cohort of patients with relapsed/refractory T-ALL, *FIP1L1-PDGFRA* fusion was identified in 14% of the patients. Identification of *FIP1L1-PDGFRA* fusion in two of our reported patients led to integration of targeted therapy, with possibly improved outcomes. *FIP1L1-PDGFRA* fusion has been reported in a few cases of T-ALL associated with eosinophilia (26,62), unlike

Author Manuscript Author Manuscript Author Manuscript Author Manuscript

our patients who did not have findings of eosinophilia. Analysis of the TARGET T-ALL data (13) identified a single case (PATBGC) of a 3-way translocation involving *PDGFRA*. TARGET T-ALL data has excluded patients with refractory T-ALL, as a remission sample was used for a germline DNA source. Based on our data, *FIP1L1-PDGFRA* fusions may be recurrent in patients with refractory T-ALL, highlighting the need for genomic characterization to identify these fusions. The presence of this fusion in T-ALL and T-LBL highlights the possibility of lineage-independent discovery of targetable alterations and the utility of tissue-agnostic clinical trials for well-characterized molecular targets. With increased integration of genomics into standard clinical care, early identification of targetable alterations may improve long-term outcomes.

Development and integration of clinical genomics assays will continue to inform incorporation of targeted therapies. *FIP1L1-PDGFRA* fusions are traditionally found using a FISH assay, requiring a priori clinical suspicion to prompt ordering this test. In patient 146, a DNA-based panel sequencing assay found loss of reads over 5' targeted regions of *PDGFRA*, raising suspicion for the presence of a *PDGFRA* fusion. An RNA-based fusion assay confirmed the presence of the *FIP1L1-PDGFRA* fusion. We used PDX cells to perform RNASeq to find the presence of the *PDGFRA* p.D842N mutation on the same transcript as the *FIP1L1-PDGFRA* fusion. Interestingly, the fusion was not detected in RNASeq using multiple fusion detector algorithms but was seen on manual review of the RNASeq data. Discrepancy between targeted fusion detection and RNASeq has been reported for solid tumors (63). Thus, clinical integration of more broad and unbiased sequencing, such as RNASeq or whole exome/whole genome sequencing (WGS), may not always be superior to the depth of sequencing permitted by targeted panels. Integration of WGS with RNASeq may be necessary to detect more complex rearrangements, such as the three-way translocation seen in TARGET patient PATBGC.

Most kinase inhibitors compete with ATP for the active site of the protein. TKI resistance mutations can prevent drug binding by altering the structure of the kinase domain and the balance between active and inactive kinase states. These mutations may arise in *de novo* disease or during therapy with a targeted inhibitor, preventing effective use of a TKI. *PDGFRA* p.D842V leads to constitutive activation of PDGFRA and is the most common mutation associated with imatinib resistance (24). The leukemia of patient 146 harbored a *PDGFRA* p.D842N mutation, though its significance was unknown. We utilized molecular dynamics and free energy calculations to model the effects of *PDGFRA* D842 substitution mutations on PDGFRA activation. We found that all profiled position 842 mutations demonstrated free energy changes predicted to be activating. The currently available algorithms to predict the significance of VUSs are inconsistent and are frequently incorrect (64). These methods predict the impact of a mutation based on physiochemical properties, evolutionary conservation and/or static structural data, and largely focus on the single amino acid that is mutated (64). In contrast, molecular dynamics is a method that uses Newton's Laws of Motion to evaluate dynamic changes in every atom of mutated protein and can accurately predict conformational changes that result from changes in a protein (65). This technique has been used in the past to understand the impact of cancer-causing kinase mutations (66). However, to our knowledge, using molecular dynamics and free energy calculations based on simulations to predict the impact of a patient mutation has not

Author Manuscript Author Manuscript Author Manuscript Author Manuscript

previously been reported. These techniques have the potential to be combined with current algorithms to improve our ability to predict the impact of VUSs on kinases.

Using a Ba/F3 IL-3 independence assay, we confirmed the activating nature of all tested D842 mutations (p.D842N, p.D842H, p.D842E, p.D842Q, p.D842T). Patient A1 had *PDGFRA* p.R383C mutation in the extracellular domain of PDGFRA. This mutation was not activating in a Ba/F3 IL-3 withdrawal assay, underscoring the importance of mutation testing/validation to inform potential clinical impact. Understanding the protein structure and possibility of resistance mutations is critical to long-term use of tyrosine kinase inhibitors. Expeditious use of targeted therapy will require knowledge about kinase structure and mutations to allow for rapid implementation of targeted therapy for patients with aggressive disease such as acute leukemia.

The tested D842 mutations showed variable sensitivity to TKIs, providing insight into the clinical use of specific inhibitors. The D842V mutation is known to render resistance to imatinib but has been reported to be sensitive to dasatinib *in vitro* (67). The relative sensitivity to imatinib between D842V and D842N may be related to the time that the mutant protein is in the active versus inactive state. This is consistent with our molecular dynamics simulations and free energy calculations. Mutation-dependent TKI sensitivity has been seen for *FLT3* mutations where *FLT3* D835Y/V/I/F showed resistance to type 2 TKIs, while D835N/E/G/A retained relative sensitivity to type 2 FLT3 TKI (68).

Dasatinib has been found to be active in T-ALL, likely due to its inhibition of LCK, suggesting potential clinical utility of dasatinib for patients with T-ALL irrespective of the presence of an activating *PDGFRA* mutation (18,69). Interestingly, Patient 146 demonstrated frank disease progression while receiving dasatinib therapy, suggesting that LCK inhibition was insufficient to prevent disease progression in this highly refractory disease. The response to avapritinib suggests that targeting PDGFRA over LCK was key to inhibiting this disease. It is possible that the concurrent mutations, *FIP1L1-PDGFRA* and *PDGFRA* p.D842N, rendered dasatinib resistance as has been previously seen with the combination of *FIP1L1-PDGFRA* and *PDGFRA* p.D842V (25). This further highlights the need for systematic identification and validation of novel mutations to inform patient treatment.

Avapritinib is a highly selective kinase inhibitor of KIT and PDGFRA. It was initially approved by the FDA for treatment of GIST, followed by approval for treatment of advanced systemic mastocytosis and related disorders (29). We report patient 146 as the first patient to receive avapritinib for T-ALL. She received avapritinib for a total of 48 days and experienced clinical benefit as evidenced by a significant decrease in bone marrow leukemia burden. This supports further development of tissue type agnostic clinical trials driven by biomarker selection and further development of avapritinib for treatment of acute leukemia.

Using a PDX model developed from patient 146's leukemia, we tested the activity of avapritinib *in vivo* to further inform patient response and possible resistance. All mice in the treatment group responded to avapritinib. Three of the five treated mice had recurrent disease after avapritinib was discontinued. In these mice, re-treatment with avapritinib

Author Manuscript Author Manuscript Author Manuscript Author Manuscript

demonstrated continued efficacy without clear evidence of resistance to this drug. Notably, two mice were cured after 28 days of avapritinib with disease-free survival at >350 days. Sequential and longer treatment in similar models may help determine therapy resistance and future optimization of kinase inhibitors.

Continued integration of genomic profiling into the care of patients with leukemia and other cancers will identify targetable alterations and possible use of targeted therapies. Increasingly patients will be treated with targeted therapy off trial, especially with approved therapies that may be available for the target but for an alternative indication. While molecularly defined basket trials and genomic profiling studies present the opportunity to understand response to therapy for patients eligible and able to enroll on trials, there is a critical need to comprehensively collect and report response data for those patients treated off trial to inform the ongoing use of these agents. With increased sequencing, additional mutations of unknown significance will be discovered, highlighting the need for pipelines to inform mutation pathogenicity and validation.

## Supplementary Material

Refer to Web version on PubMed Central for supplementary material.

## Acknowledgments

This work is supported by a St. Baldrick's Foundation Consortium grant and Hannah's Heroes. This work was supported by the following grants from the National Institutes of Health (NIH)/National Cancer Institute (NCI): R35 CA210030 (KS), NCI R35 CA197695 (CGM), K08 CA222684 (YP), and 5T32HL007574–38 (JP). This work was additionally supported by Team Crank (KS), the American Lebanese Syrian Associated Charities of St Jude Children's Research Hospital (CGM), and the Children's Leukemia Research Association (KS). SKT is a Scholar of the Leukemia & Lymphoma Society and holds the Joshua Kahan Endowed Chair in Pediatric Leukemia Research at the Children's Hospital of Philadelphia.

## References

1. Pikman Y, Tasian SK, Sulis ML, Stevenson K, Blonquist TM, Apsel Winger B, et al. Matched Targeted Therapy for Pediatric Patients with Relapsed, Refractory, or High-Risk Leukemias: A Report from the LEAP Consortium. Cancer Discov 2021;11(6):1424–39 doi 10.1158/2159-8290.Cd-20-0564. [PubMed: 33563661]
2. Harris MH, DuBois SG, Glade Bender JL, Kim A, Crompton BD, Parker E, et al. Multicenter Feasibility Study of Tumor Molecular Profiling to Inform Therapeutic Decisions in Advanced Pediatric Solid Tumors: The Individualized Cancer Therapy (iCat) Study. JAMA Oncology 2016;2(5):608–15 doi 10.1001/jamaoncol.2015.5689. [PubMed: 26822149]
3. Rapport F, Smith J, O'Brien TA, Tyrrell VJ, Mould EV, Long JC, et al. Development of an implementation and evaluation strategy for the Australian 'Zero Childhood Cancer' (Zero) Program: a study protocol. BMJ Open 2020;10(6):e034522 doi 10.1136/bmjopen-2019-034522.
4. Massard C, Michiels S, Ferté C, Le Deley M-C, Lacroix L, Hollebecque A, et al. High-Throughput Genomics and Clinical Outcome in Hard-to-Treat Advanced Cancers: Results of the MOSCATO 01 Trial. Cancer Discovery 2017;7(6):586–95 doi 10.1158/2159-8290.Cd-16-1396. [PubMed: 28365644]
5. George SL, Izquierdo E, Campbell J, Koutroumanidou E, Proszek P, Jamal S, et al. A tailored molecular profiling programme for children with cancer to identify clinically actionable genetic alterations. Eur J Cancer 2019;121:224–35 doi 10.1016/j.ejca.2019.07.027. [PubMed: 31543384]

Author Manuscript Author Manuscript Author Manuscript Author Manuscript


6. Langenberg K, Dolman E, Molenaar J. Abstract A40: Integration of high-throughput drug screening on patient-derived organdies into pediatric precision medicine programs: The future is now! Cancer Research 2020;80(14 Supplement):A40–A doi 10.1158/1538-7445.Pedca19-a40.
7. Berlanga P, Pierron G, Lacroix L, Chicard M, Adam de Beaumais T, Marchais A, et al. The European MAPPYACTS trial: Precision Medicine Program in Pediatric and Adolescent Patients with Recurrent Malignancies. Cancer Discov 2022 doi 10.1158/2159-8290.Cd-21-1136.
8. van Tilburg CM, Pfaff E, Pajtler KW, Langenberg KPS, Fiesel P, Jones BC, et al. The Pediatric Precision Oncology INFORM Registry: Clinical Outcome and Benefit for Patients with Very High-Evidence Targets. Cancer Discov 2021;11(11):2764–79 doi 10.1158/2159-8290.CD-21-0094. [PubMed: 34373263]
9. Parsons DW, Janeway KA, Patton DR, Winter CL, Coffey B, Williams PM, et al. Actionable Tumor Alterations and Treatment Protocol Enrollment of Pediatric and Young Adult Patients With Refractory Cancers in the National Cancer Institute-Children's Oncology Group Pediatric MATCH Trial. J Clin Oncol 2022;40(20):2224–34 doi 10.1200/jco.21.02838. [PubMed: 35353553]
10. Burd A, Levine RL, Ruppert AS, Mims AS, Borate U, Stein EM, et al. Precision medicine treatment in acute myeloid leukemia using prospective genomic profiling: feasibility and preliminary efficacy of the Beat AML Master Trial. Nat Med 2020;26(12):1852–8 doi 10.1038/s41591-020-1089-8. [PubMed: 33106665]
11. Girardi T, Vicente C, Cools J, De Keersmaecker K. The genetics and molecular biology of T-ALL. Blood 2017;129(9):1113–23 doi 10.1182/blood-2016-10-706465. [PubMed: 28115373]
12. Khanam T, Sandmann S, Seggewiss J, Ruether C, Zimmermann M, Norvil AB, et al. Integrative genomic analysis of pediatric T-cell lymphoblastic lymphoma reveals candidates of clinical significance. Blood 2021;137(17):2347–59 doi 10.1182/blood.2020005381. [PubMed: 33152759]
13. Brady SW, Roberts KG, Gu Z, Shi L, Pounds S, Pei D, et al. The genomic landscape of pediatric acute lymphoblastic leukemia. Nat Genet 2022;54(9):1376–89 doi 10.1038/s41588-022-01159-z. [PubMed: 36050548]
14. Liu Y, Easton J, Shao Y, Maciaszek J, Wang Z, Wilkinson MR, et al. The genomic landscape of pediatric and young adult T-lineage acute lymphoblastic leukemia. Nat Genet 2017;49(8):1211–8 doi 10.1038/ng.3909. [PubMed: 28671688]
15. Gianfelici V, Chiaretti S, Demeyer S, Di Giacomo F, Messina M, La Starza R, et al. RNA sequencing unravels the genetics of refractory/relapsed T-cell acute lymphoblastic leukemia. Prognostic and therapeutic implications. Haematologica 2016;101(8):941–50 doi 10.3324/haematol.2015.139410. [PubMed: 27151993]
16. Richter-Pechańska P, Kunz JB, Rausch T, Erarslan-Uysal B, Bornhauser B, Frismantas V, et al. Pediatric T-ALL type-1 and type-2 relapses develop along distinct pathways of clonal evolution. Leukemia 2022;36(7):1759–68 doi 10.1038/s41375-022-01587-0. [PubMed: 35585141]
17. Cordo V, van der Zwet JCG, Canté-Barrett K, Pieters R, Meijerink JPP. T-cell Acute Lymphoblastic Leukemia: A Roadmap to Targeted Therapies. Blood Cancer Discov 2021;2(1):19–31 doi 10.1158/2643-3230.Bcd-20-0093. [PubMed: 34661151]
18. Laukkanen S, Veloso A, Yan C, Oksa L, Alpert EJ, Do D, et al. Therapeutic targeting of LCK tyrosine kinase and mTOR signaling in T-cell acute lymphoblastic leukemia. Blood 2022;140(17):1891–906 doi 10.1182/blood.2021015106. [PubMed: 35544598]
19. Mamonkin M, Rouce RH, Tashiro H, Brenner MK. A T-cell-directed chimeric antigen receptor for the selective treatment of T-cell malignancies. Blood 2015;126(8):983–92 doi 10.1182/blood-2015-02-629527. [PubMed: 26056165]
20. Schrappe M, Hunger SP, Pui CH, Saha V, Gaynon PS, Baruchel A, et al. Outcomes after induction failure in childhood acute lymphoblastic leukemia. N Engl J Med 2012;366(15):1371–81 doi 10.1056/NEJMoa1110169. [PubMed: 22494120]
21. Andrae J, Gallini R, Betsholtz C. Role of platelet-derived growth factors in physiology and medicine. Genes Dev 2008;22(10):1276–312 doi 10.1101/gad.1653708. [PubMed: 18483217]
22. Klug LR, Kent JD, Heinrich MC. Structural and clinical consequences of activation loop mutations in class III receptor tyrosine kinases. Pharmacol Ther 2018;191:123–34 doi 10.1016/j.pharmthera.2018.06.016. [PubMed: 29964125]

Author Manuscript Author Manuscript Author Manuscript Author Manuscript


23. Cools J, DeAngelo DJ, Gotlib J, Stover EH, Legare RD, Cortes J, et al. A tyrosine kinase created by fusion of the PDGFRA and FIP1L1 genes as a therapeutic target of imatinib in idiopathic hypereosinophilic syndrome. N Engl J Med 2003;348(13):1201–14 doi 10.1056/NEJMoa025217. [PubMed: 12660384]
24. Corless CL, Schroeder A, Griffith D, Town A, McGreevey L, Harrell P, et al. PDGFRA mutations in gastrointestinal stromal tumors: frequency, spectrum and in vitro sensitivity to imatinib. J Clin Oncol 2005;23(23):5357–64 doi 10.1200/jco.2005.14.068. [PubMed: 15928335]
25. Lierman E, Michaux L, Beullens E, Pierre P, Marynen P, Cools J, et al. FIP1L1-PDGFRalpha D842V, a novel panresistant mutant, emerging after treatment of FIP1L1-PDGFRalpha T674I eosinophilic leukemia with single agent sorafenib. Leukemia 2009;23(5):845–51 doi 10.1038/leu.2009.2. [PubMed: 19212337]
26. Oberley MJ, Denton C, Ji J, Hiemenz M, Bhojwani D, Ostrow D, et al. A neoplasm with FIP1L1-PDGFRA fusion presenting as pediatric T-cell lymphoblastic leukemia/lymphoma without eosinophilia. Cancer Genet 2017;216-217:91–9 doi 10.1016/j.cancergen.2017.07.007. [PubMed: 29025601]
27. Evans EK, Gardino AK, Kim JL, Hodous BL, Shutes A, Davis A, et al. A precision therapy against cancers driven by KIT/PDGFRA mutations. Sci Transl Med 2017;9(414) doi 10.1126/scitranslmed.aao1690.
28. Heinrich MC, Jones RL, von Mehren M, Schöffski P, Serrano C, Kang YK, et al. Avapritinib in advanced PDGFRA D842V-mutant gastrointestinal stromal tumour (NAVIGATOR): a multicentre, open-label, phase 1 trial. Lancet Oncol 2020;21(7):935–46 doi 10.1016/s1470-2045(20)30269-2. [PubMed: 32615108]
29. Gotlib J, Reiter A, Radia DH, Deininger MW, George TI, Panse J, et al. Efficacy and safety of avapritinib in advanced systemic mastocytosis: interim analysis of the phase 2 PATHFINDER trial. Nat Med 2021;27(12):2192–9 doi 10.1038/s41591-021-01539-8. [PubMed: 34873345]
30. Burns MA, Place AE, Stevenson KE, Gutiérrez A, Forrest S, Pikman Y, et al. Identification of prognostic factors in childhood T-cell acute lymphoblastic leukemia: Results from DFCI ALL Consortium Protocols 05-001 and 11-001. Pediatr Blood Cancer 2021;68(1):e28719 doi 10.1002/pbc.28719. [PubMed: 33026184]
31. Yin J, Zhu F, Zhang ZB, Wang Q, He XF, Wu Q, et al. Rapid and deep response to avapritinib in heavily treated acute myeloid leukemia with t (8;21) and KIT mutation. Ann Hematol 2022;101(10):2347–50 doi 10.1007/s00277-022-04897-6. [PubMed: 35767050]
32. Xue S, Huang W, Liu F, Zhang Y, Hao Q, Cui B, et al. Rapid response to avapritinib of acute myeloid leukemia with t(8;21) and KIT mutation relapse post allo-HSCT. Leuk Lymphoma 2022;63(9):2247–50 doi 10.1080/10428194.2022.2064994. [PubMed: 35440293]
33. Walz C, Score J, Mix J, Cilloni D, Roche-Lestienne C, Yeh RF, et al. The molecular anatomy of the FIP1L1-PDGFRA fusion gene. Leukemia 2009;23(2):271–8 doi 10.1038/leu.2008.310. [PubMed: 18987651]
34. Gotlib J, Cools J, Malone JM 3rd, Schrier SL, Gilliland DG, Coutré SE. The FIP1L1-PDGFRalpha fusion tyrosine kinase in hypereosinophilic syndrome and chronic eosinophilic leukemia: implications for diagnosis, classification, and management. Blood 2004;103(8):2879–91 doi 10.1182/blood-2003-06-1824. [PubMed: 15070659]
35. Metzgeroth G, Walz C, Score J, Siebert R, Schnittger S, Haferlach C, et al. Recurrent finding of the FIP1L1-PDGFRA fusion gene in eosinophilia-associated acute myeloid leukemia and lymphoblastic T-cell lymphoma. Leukemia 2007;21(6):1183–8 doi 10.1038/sj.leu.2404662. [PubMed: 17377585]
36. Khoury JD, Solary E, Abla O, Akkari Y, Alaggio R, Apperley JF, et al. The 5th edition of the World Health Organization Classification of Haematolymphoid Tumours: Myeloid and Histiocytic/Dendritic Neoplasms. Leukemia 2022;36(7):1703–19 doi 10.1038/s41375-022-01613-1. [PubMed: 35732831]
37. Kluk MJ, Lindsley RC, Aster JC, Lindeman NI, Szeto D, Hall D, et al. Validation and Implementation of a Custom Next-Generation Sequencing Clinical Assay for Hematologic Malignancies. J Mol Diagn 2016;18(4):507–15 doi 10.1016/j.jmoldx.2016.02.003. [PubMed: 27339098]

Author Manuscript Author Manuscript Author Manuscript Author Manuscript


38. Garcia EP, Minkovsky A, Jia Y, Ducar MD, Shivdasani P, Gong X, et al. Validation of OncoPanel: A Targeted Next-Generation Sequencing Assay for the Detection of Somatic Variants in Cancer. Arch Pathol Lab Med 2017;141(6):751–8 doi 10.5858/arpa.2016-0527-OA. [PubMed: 28557599]
39. Liang L, Yan XE, Yin Y, Yun CH. Structural and biochemical studies of the PDGFRA kinase domain. Biochem Biophys Res Commun 2016;477(4):667–72 doi 10.1016/j.bbrc.2016.06.117. [PubMed: 27349873]
40. Gapsys V, de Groot BL. pmx Webserver: A User Friendly Interface for Alchemistry. J Chem Inf Model 2017;57(2):109–14 doi 10.1021/acs.jcim.6b00498. [PubMed: 28181802]
41. Maier JA, Martinez C, Kasavajhala K, Wickstrom L, Hauser KE, Simmerling C. ff14SB: Improving the Accuracy of Protein Side Chain and Backbone Parameters from ff99SB. J Chem Theory Comput 2015;11(8):3696–713 doi 10.1021/acs.jctc.5b00255. [PubMed: 26574453]
42. Joung IS, Cheatham TE 3rd. Determination of alkali and halide monovalent ion parameters for use in explicitly solvated biomolecular simulations. J Phys Chem B 2008;112(30):9020–41 doi 10.1021/jp8001614. [PubMed: 18593145]
43. Jorgensen WL, Chandrasekhar J, Madura JD, Impey RW, Klein ML. Comparison of simple potential functions for simulating liquid water. The Journal of Chemical Physics 1983;79(2):926–35 doi 10.1063/1.445869.
44. Essmann U, Perera L, Berkowitz ML, Darden T, Lee H, Pedersen LG. A smooth particle mesh Ewald method. The Journal of Chemical Physics 1995;103(19):8577–93 doi 10.1063/1.470117.
45. Hess B, Bekker H, Berendsen HJC, Fraaije JGEM. LINCS: A linear constraint solver for molecular simulations. Journal of Computational Chemistry 1997;18(12):1463–72 doi 10.1002/(SICI)1096-987X(199709)18:12<1463::AID-JCC4>3.0.CO;2-H.
46. Miyamoto S, Kollman PA. Settle: An analytical version of the SHAKE and RATTLE algorithm for rigid water models. Journal of Computational Chemistry 1992;13(8):952–62 doi 10.1002/jcc.540130805.
47. Shirts MR, Bair E, Hooker G, Pande VS. Equilibrium Free Energies from Nonequilibrium Measurements Using Maximum-Likelihood Methods. Physical Review Letters 2003;91(14):140601 doi 10.1103/PhysRevLett.91.140601. [PubMed: 14611511]
48. Oberg JA, Glade Bender JL, Sulis ML, Pendrick D, Sireci AN, Hsiao SJ, et al. Implementation of next generation sequencing into pediatric hematology-oncology practice: moving beyond actionable alterations. Genome Med 2016;8(1):133 doi 10.1186/s13073-016-0389-6. [PubMed: 28007021]
49. O'Connor D, Demeulemeester J, Conde L, Kirkwood AA, Fung K, Papaleonidopoulou F, et al. The Clinico-Genomic Landscape of Induction Failure in Childhood and Young Adult T-Cell Acute Lymphoblastic Leukemia (T-ALL). Blood 2022;140(Supplement 1):1720–1 doi 10.1182/blood-2022-165308.
50. Dunsmore KP, Winter SS, Devidas M, Wood BL, Esiashvili N, Chen Z, et al. Children's Oncology Group AALL0434: A Phase III Randomized Clinical Trial Testing Nelarabine in Newly Diagnosed T-Cell Acute Lymphoblastic Leukemia. J Clin Oncol 2020;38(28):3282–93 doi 10.1200/jco.20.00256. [PubMed: 32813610]
51. Horton TM, Lu X, O'Brien MM, Borowitz MJ, Devidas M, Raetz EA, et al. Bortezomib reinduction therapy to improve response rates in pediatric ALL in first relapse: A Children's Oncology Group (COG) study (AALL07P1). Journal of Clinical Oncology 2013;31(15_suppl):10003- doi 10.1200/jco.2013.31.15_suppl.10003.
52. Teachey DT, Devidas M, Wood BL, Chen Z, Hayashi RJ, Hermiston ML, et al. Children's Oncology Group Trial AALL1231: A Phase III Clinical Trial Testing Bortezomib in Newly Diagnosed T-Cell Acute Lymphoblastic Leukemia and Lymphoma. J Clin Oncol 2022;40(19):2106–18 doi 10.1200/jco.21.02678. [PubMed: 35271306]
53. Wilson WH, Grossbard ML, Pittaluga S, Cole D, Pearson D, Drbohlav N, et al. Dose-adjusted EPOCH chemotherapy for untreated large B-cell lymphomas: a pharmacodynamic approach with high efficacy. Blood 2002;99(8):2685–93 doi 10.1182/blood.v99.8.2685. [PubMed: 11929754]
54. Stock W, Luger SM, Advani AS, Yin J, Harvey RC, Mullighan CG, et al. A pediatric regimen for older adolescents and young adults with acute lymphoblastic leukemia: results of CALGB 10403. Blood 2019;133(14):1548–59 doi 10.1182/blood-2018-10-881961. [PubMed: 30658992]

Author Manuscript Author Manuscript Author Manuscript Author Manuscript


55. Larsen EC, Devidas M, Chen S, Salzer WL, Raetz EA, Loh ML, et al. Dexamethasone and High-Dose Methotrexate Improve Outcome for Children and Young Adults With High-Risk B-Acute Lymphoblastic Leukemia: A Report From Children's Oncology Group Study AALL0232. J Clin Oncol 2016;34(20):2380–8 doi 10.1200/JCO.2015.62.4544. [PubMed: 27114587]
56. Kawagishi J, Kumabe T, Yoshimoto T, Yamamoto T. Structure, organization, and transcription units of the human alpha-platelet-derived growth factor receptor gene, PDGFRA. Genomics 1995;30(2):224–32 doi 10.1006/geno.1995.9883. [PubMed: 8586421]
57. Haas BJ, Dobin A, Li B, Stransky N, Pochet N, Regev A. Accuracy assessment of fusion transcript detection via read-mapping and de novo fusion transcript assembly-based methods. Genome Biology 2019;20(1):213 doi 10.1186/s13059-019-1842-9. [PubMed: 31639029]
58. Rodríguez-Martín B, Palumbo E, Marco-Sola S, Griebel T, Ribeca P, Alonso G, et al. ChimPipe: accurate detection of fusion genes and transcription-induced chimeras from RNA-seq data. BMC Genomics 2017;18(1):7 doi 10.1186/s12864-016-3404-9. [PubMed: 28049418]
59. Nicorici D, Satalan M, Edgren H, Kangaspeska S, Murumagi A, Kallioniemi O, et al. FusionCatcher - a tool for finding somatic fusion genes in paired-end RNA-sequencing data. 2014.
60. Roberts KG, Li Y, Payne-Turner D, Harvey RC, Yang YL, Pei D, et al. Targetable kinase-activating lesions in Ph-like acute lymphoblastic leukemia. N Engl J Med 2014;371(11):1005–15 doi 10.1056/NEJMoa1403088. [PubMed: 25207766]
61. Schultz KR, Carroll A, Heerema NA, Bowman WP, Aledo A, Slayton WB, et al. Long-term follow-up of imatinib in pediatric Philadelphia chromosome-positive acute lymphoblastic leukemia: Children's Oncology Group study AALL0031. Leukemia 2014;28(7):1467–71 doi 10.1038/leu.2014.30. [PubMed: 24441288]
62. Metzgeroth G, Walz C, Score J, Siebert R, Schnittger S, Haferlach C, et al. Recurrent finding of the FIP1L1-PDGFRA fusion gene in eosinophilia-associated acute myeloid leukemia and lymphoblastic T-cell lymphoma. Leukemia 2007;21(6):1183–8 doi 10.1038/sj.leu.2404662. [PubMed: 17377585]
63. Church AJ, Corson LB, Kao PC, Imamovic-Tuco A, Reidy D, Doan D, et al. Molecular profiling identifies targeted therapy opportunities in pediatric solid cancer. Nat Med 2022 doi 10.1038/s41591-022-01856-6.
64. Schulz WL, Tormey CA, Torres R. Computational Approach to Annotating Variants of Unknown Significance in Clinical Next Generation Sequencing. Lab Med 2015;46(4):285–9 doi 10.1309/LMWZH57BRWOPR5RQ. [PubMed: 26489672]
65. Karplus M, McCammon JA. Molecular dynamics simulations of biomolecules. Nat Struct Biol 2002;9(9):646–52 doi 10.1038/nsb0902-646. [PubMed: 12198485]
66. White KA, Ruiz DG, Szpiech ZA, Strauli NB, Hernandez RD, Jacobson MP, et al. Cancer-associated arginine-to-histidine mutations confer a gain in pH sensing to mutant proteins. Sci Signal 2017;10(495) doi 10.1126/scisignal.aam9931.
67. Dewaele B, Wasag B, Cools J, Sciot R, Prenen H, Vandenberghe P, et al. Activity of dasatinib, a dual SRC/ABL kinase inhibitor, and IPI-504, a heat shock protein 90 inhibitor, against gastrointestinal stromal tumor-associated PDGFRAD842V mutation. Clin Cancer Res 2008;14(18):5749–58 doi 10.1158/1078-0432.Ccr-08-0533. [PubMed: 18794084]
68. Smith CC, Lin K, Stecula A, Sali A, Shah NP. FLT3 D835 mutations confer differential resistance to type II FLT3 inhibitors. Leukemia 2015;29(12):2390–2 doi 10.1038/leu.2015.165. [PubMed: 26108694]
69. Frismantas V, Dobay MP, Rinaldi A, Tchinda J, Dunn SH, Kunz J, et al. Ex vivo drug response profiling detects recurrent sensitivity patterns in drug-resistant acute lymphoblastic leukemia. Blood 2017;129(11):e26–e37 doi 10.1182/blood-2016-09-738070. [PubMed: 28122742]

Author Manuscript Author Manuscript Author Manuscript Author Manuscript

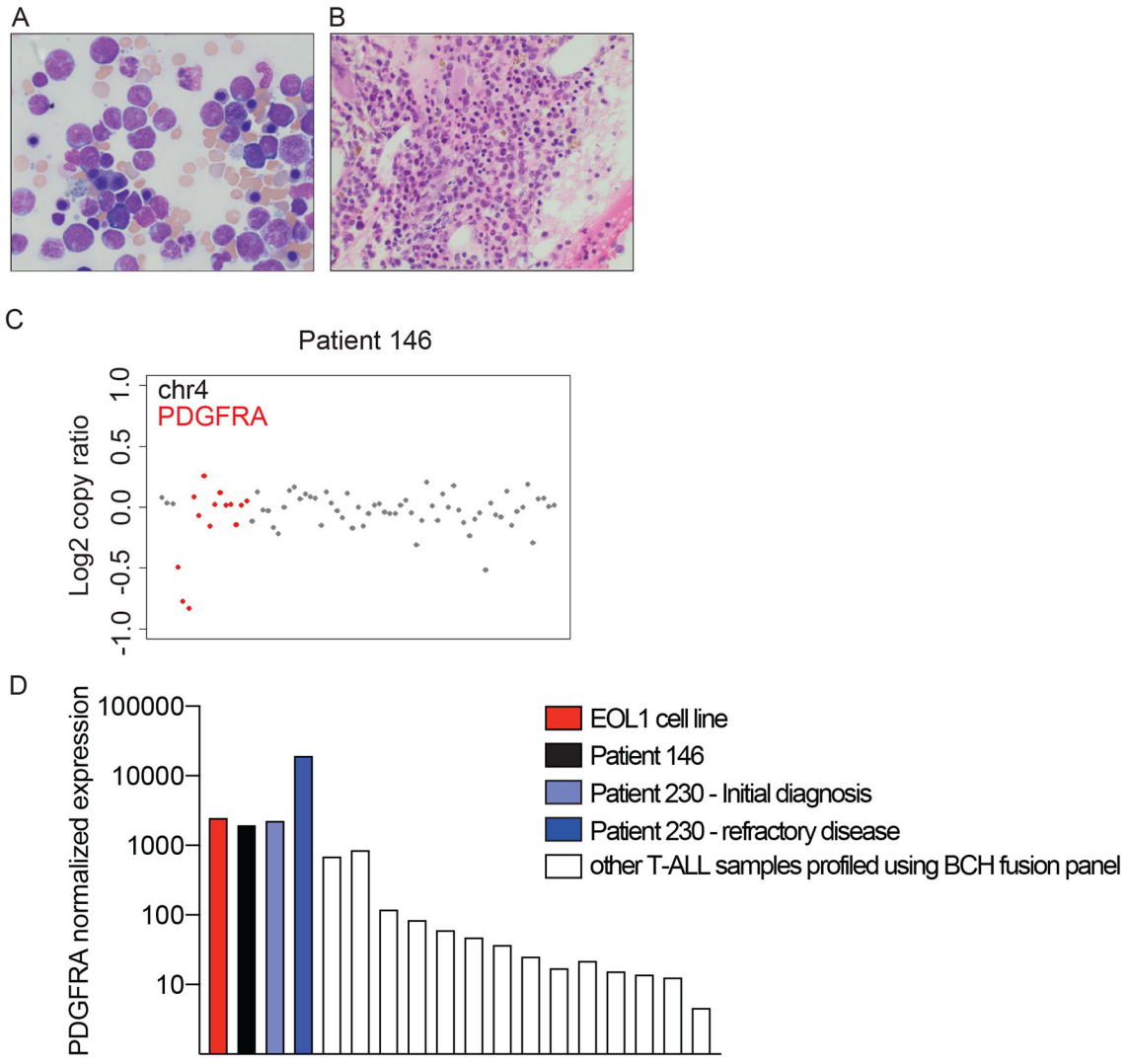


**Figure 1:**

Clinical pathology for pediatric T-ALL patients. A. Bone marrow smear from patient 146, stained with hematoxylin and eosin (H&E) stains. Shown is a representative field with image taken at 100X magnification. B. Histology of bone marrow biopsy core from patient 146. Shown is a representative section stained with H&E. Image was taken at 60X magnification. C. Graph showing read counts for probes along chromosome 4 on the RHP v2 assay (Batch CNV) for bone marrow from patient 146. Red highlights amplicons for *PDGFRA* (exons 10-21 and 23) and demonstrates loss of reads over exons 10-12, suggesting deletion of a 5' segment of *PDGFRA*. Shown are data from one of two sample replicates. D. Graph showing *PDGFRA* expression for T-ALL samples and the EOL1 cell line analyzed using the AMPSeq fusion assay. *PDGFRA* expression is calculated as number of reads/million total RNA reads. T-ALL samples include all clinical disease samples profiled using the Boston Children's Hospital AMPSeq fusion panel between July 2020- November 2021.

Author Manuscript Author Manuscript Author Manuscript Author Manuscript

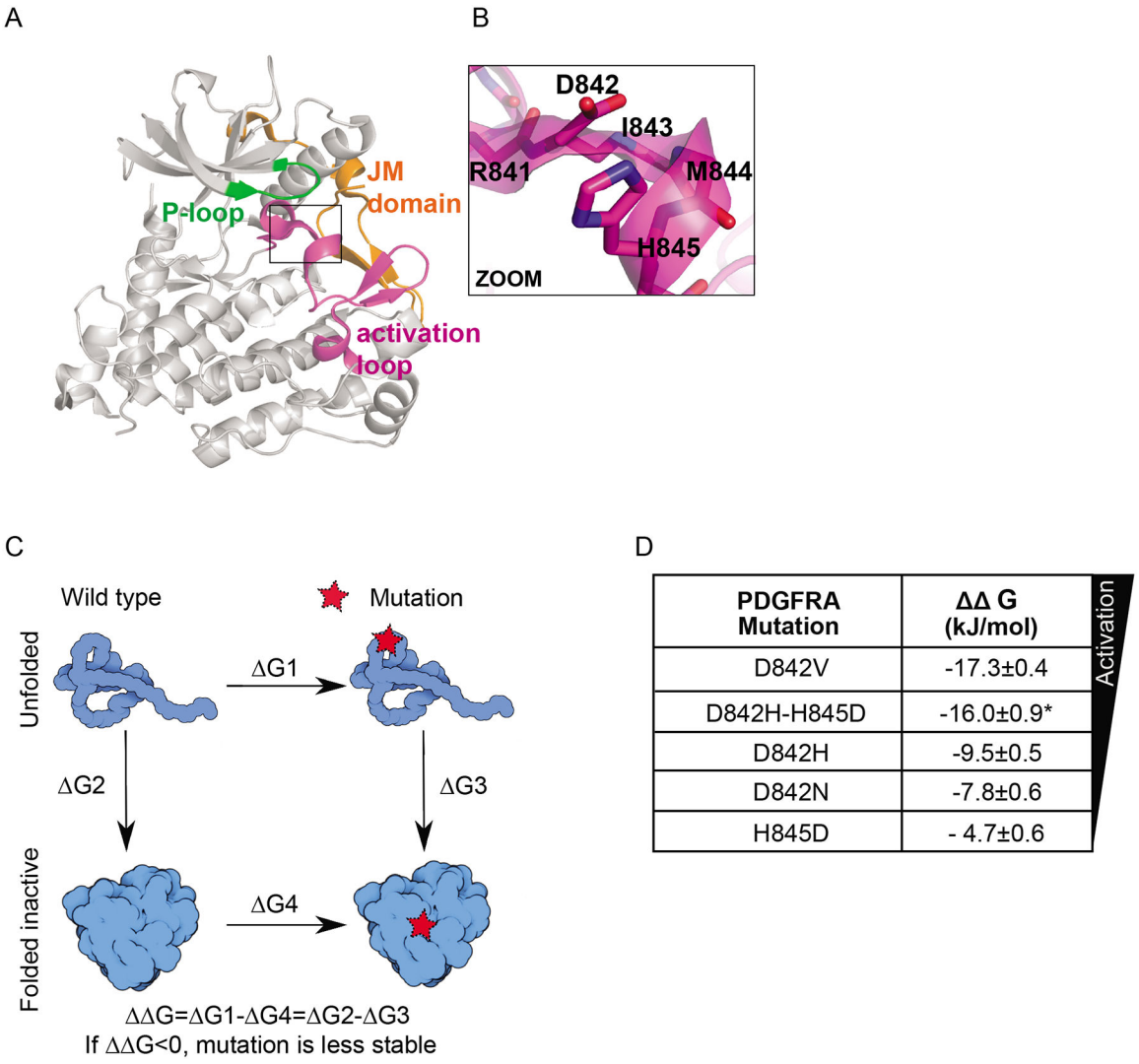


**Figure 2:**

Alchemical free energy calculations predict activation by *PDGFRA* p.D842X mutants. A. Crystallographic structure of PDGFRA. B. Zoom of the crystal structure around the D842 residue. C. Schematic representation of the thermodynamic cycle of wildtype and mutant PDGFRA in the unfolded and folded, auto-inhibited state. *For the schematic representation of the double mutant D842H/H845D, see Supplementary Figure 1A-B. D. Summary of free energy differences (ΔΔG values).

Author Manuscript Author Manuscript Author Manuscript Author Manuscript

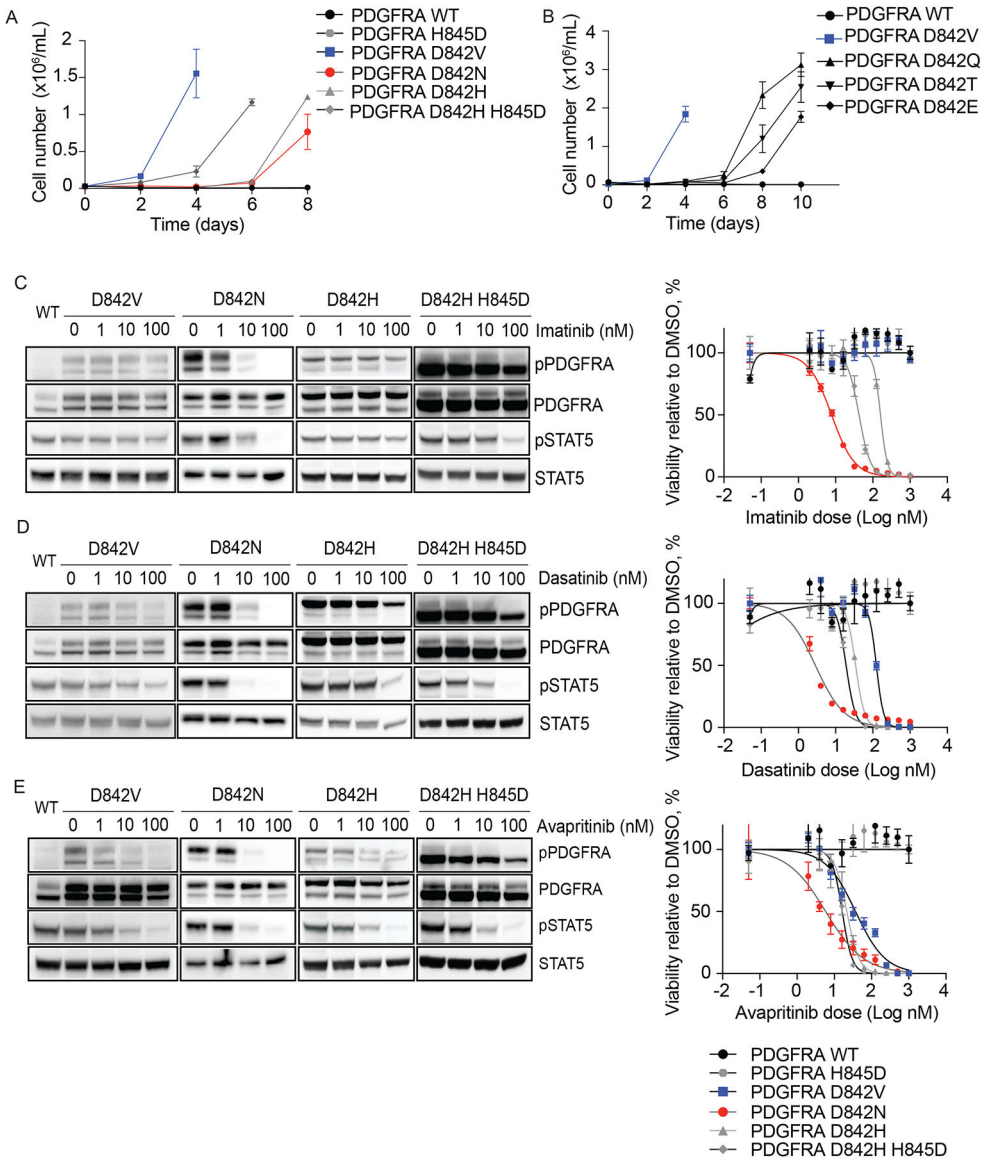


**Figure 3:**

*PDGFRA* D842 mutations result in activated PDGFRA, IL-3 independent growth, and sensitivity to tyrosine kinase inhibitors. A. Ba/F3 cells expressing *PDGFRA* WT, p.D842V, p.D842N, p.D842H, p.H845D, p.D842H/p.H845D were grown without IL-3, and cells counted using trypan blue exclusion. Shown is the average number of cells ± SD of 3 replicates. B. Ba/F3 cells expressing *PDGFRA* WT, p.D842V, p.D842Q, p.D842T, and p.D842E were grown without IL-3, and cells counted using trypan blue exclusion. Shown is the average number of cells ±SD of 3 replicates. C-E. Western immunoblotting showing inhibition of PDGFRA and STAT5 phosphorylation in response to imatinib (C), dasatinib (D), or avapritinib (E). Boxes indicate western blots performed separately and degree of activation cannot be compared between different blots. Ba/F3 cells expressing *PDGFRA* WT, H845D, D842V, D842N, D842H, or D842H/H845D were tested with a range of imatinib (C), dasatinib (D), or avapritinib (E) concentrations and viability evaluated at day 3

by an ATP-based assay as a percentage of luminescence relative to DMSO control. Shown are the mean ±SD of 4 replicates.

Author Manuscript Author Manuscript Author Manuscript Author Manuscript

Author Manuscript Author Manuscript Author Manuscript Author Manuscript

A B

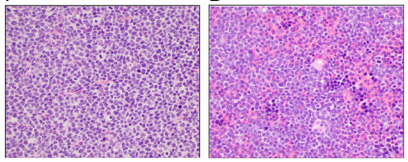

C

Immunophenotype of patient 146 and PDX model

| | Positive by flow cytometry |
|---|---|
| Patient 146 | CD2 (variable), CD5, CD7, CD8 (variable), CD99 (variable) |
| PDX | CD1a (variable), CD2, CD4 (variable), CD5, CD7 (dim), CD8, CD99 (variable) |

D

| Patient bone marrow genomic variants | | | | |
|---|---|---|---|---|
| Gene | Transcript | Genomic variant | Protein variant | VAF |
| PDGFRA | NM_006206 | c.2524G>A | p.D842N | 12.3% |
| FANCL | NM_0011114636 | c.1022_1024del | p.I341_C342delinsS | 52.4% |
| FIP1L1-PDGFRA | FIP1L1 exon 6 (NM_030917.3) :: PDGFRA exon 12 (NM_006206.4) | | | |
| STIL-TAL1 | STIL exon 1 (NM_003035.2) :: TAL1 exon 5 (NM_003189.5) | | | |
| PDX spleen genomic variants | | | | |
| Gene | Transcript | Genomic variant | Protein variant | VAF |
| PDGFRA | NM_006206 | c.2524G>A | p.D842N | 45% |
| FANCL | NM_0011114636 | c.1022_1024del | p.I341_C342delinsS | 46% |
| FIP1L1-PDGFRA | FIP1L1 exon 6 (NM_030917.3) :: PDGFRA exon 12 (NM_006206.4) | | | |
| STIL-TAL1 | STIL exon 1 (NM_003035.2) :: TAL1 exon 5 (NM_003189.5) | | | |

E F

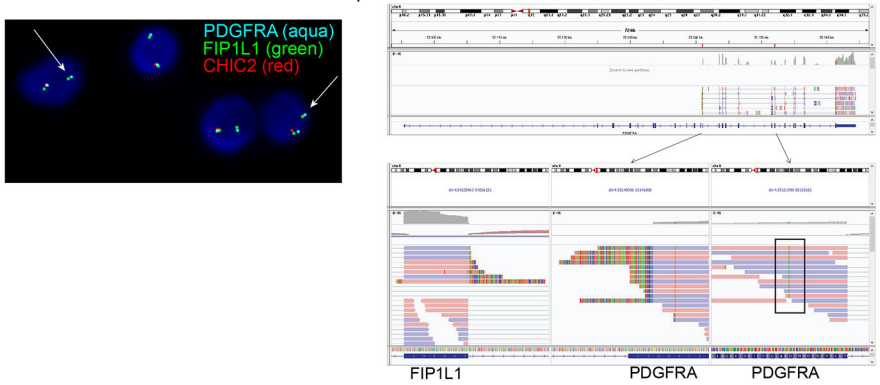


**Figure 4:**

Characterization of PDX model of *FIP1L1-PDGFRA, PDGFRA* p.D842N T-ALL from patient 1. A. Histology of mouse PDX bone marrow stained with H&E stains. Shown is a representative field with image taken at 60X magnification. B. Spleen histology of PDX model stained with H&E stains. Shown is a representative field with image taken at 60X magnification. C. Summary of flow cytometry data from patient 146 and the PDX model from patient 146. D. Table summarizing the genomic profiling results from patient 146 (data from Rapid Heme Panel and AmpSeq fusion assay) and PDX model (sequencing data from Oncopanel). Shown are data for genes that are covered on both assays. Full sequencing data from both samples are included in Supplementary Table 6. E. FISH performed in PDX spleen cells showing fusion of FIP1L1-PDGFRA, with loss of CHIC2. F. RNASeq was performed on spleen cells derived from the PDX model. Image of RNASeq alignment at the indicated area of Chromosome 4. Shown are the *PDGFRA* p.D842N mutation present

Author Manuscript Author Manuscript Author Manuscript Author Manuscript

in 100% of reads as a vertical green line (black box) in the lower right panel and the *FIP1L1-PDGFRA* fusion breakpoints in the lower left and center panels. The absence of reads over the earlier exons prior to the breakpoint in *PDGRA* exon 12 suggests that the mutant fusion allele is responsible for all of the 3' *PDGFRA* RNA expression and that the *PDGFRA* c.2524G>A p.D842N point mutation is on the same allele as the fusion.

Author Manuscript Author Manuscript Author Manuscript Author Manuscript

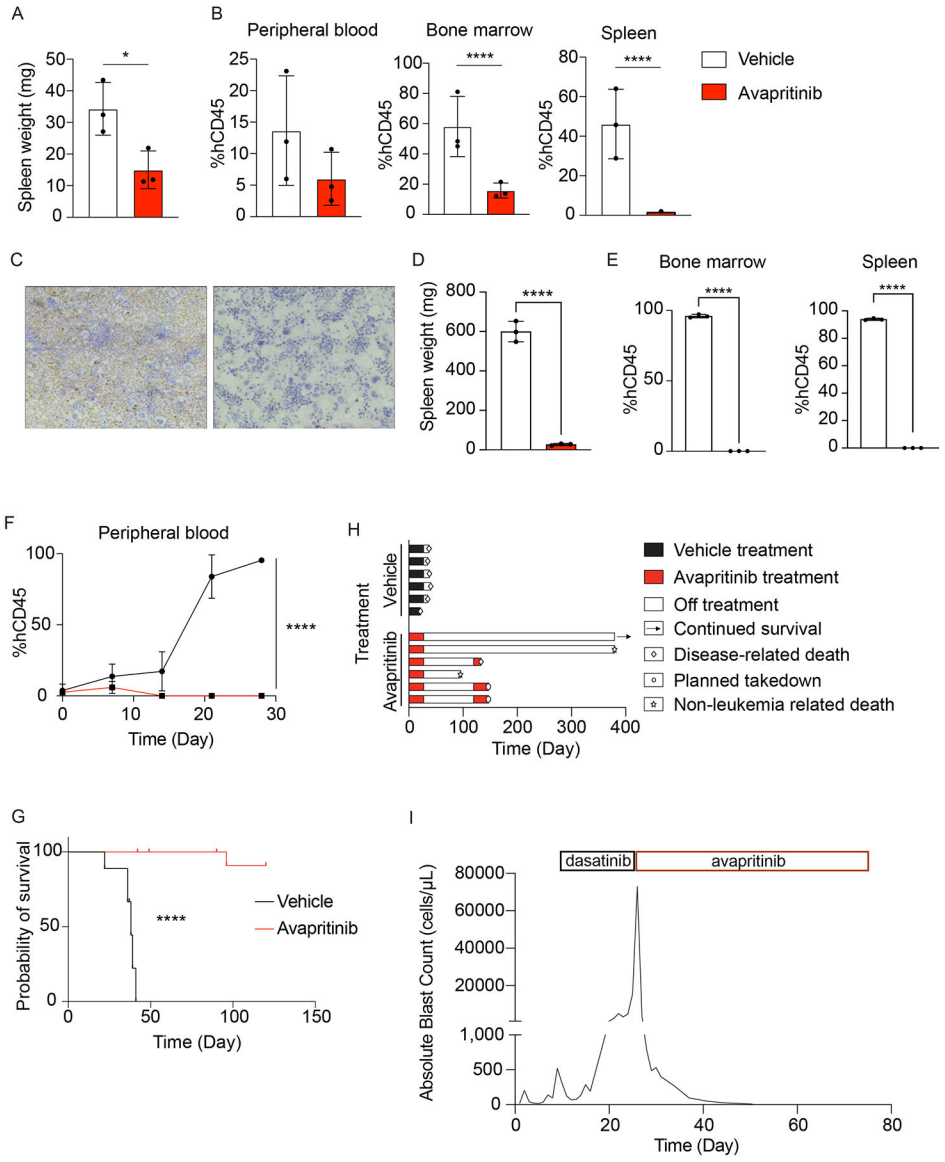


**Figure 5:**

T-ALL with *FIP1L1-PDGFRA, PDGFRA* p.D842N mutations responds to avapritinib. PDX model from patient 146, characterized by *FIP1L1-PDGFRA* and *PDGFRA* p.D842N, was treated with vehicle versus avapritinib. A. Graph showing spleen weight in mice after 7 days of treatment. Shown is average weight (n=3) ±SD. *P<0.05 using unpaired t-test. B. Avapritinib treated mice demonstrated a decrease in leukemia burden in peripheral blood, bone marrow, and spleen after 7 days of treatment. Shown are flow cytometric quantification of total human CD45+ ALL cells in harvested tissues (n=3), average ±SD. ****P<0.0001 using unpaired t-test. C. Histology of mouse bone marrow stained with pSTAT5 from mouse treated with vehicle (left) or avapritinib (right) for 7 days. Shown is a representative field with image taken at 40X magnification. Effect of avapritinib on leukemia burden was more profound after 28 days of treatment. D. Graph showing spleen weight in mice after 28 days of treatment. Shown is average weight (n=3) ±SD. ****P<0.0001 using unpaired t-test. E.

Author Manuscript Author Manuscript Author Manuscript Author Manuscript

Flow cytometric quantification of total human CD45+ ALL cells in bone marrow or spleen after 28 days of treatment. Average % human CD45 shown (n=3) ±SD. ****P<0.0001 using unpaired t-test. F. Peripheral blood leukemia was monitored in mice during treatment. Shown is average % human CD45 positive cells for 3 mice per timepoint over 28 days, ±SD. ****P<0.0001 using a 2-way ANOVA. G. Kaplan-Meier survival curve for PDX mice treated with vehicle or avapritinib. Data shown for mice that were not included in planned tissue analysis, N=6 per group. Curve for avapritinib-treated mice stops when mice with recurrent disease are re-treated with avapritinib. ****P<0.0001 using Log-rank test. H. Swimmer plot depicts complete treatment course of PDX mice treated with vehicle or avapritinib. Three mice in the avapritinib group developed disease recurrence following discontinuation of therapy and were re-treated. I. Graph showing peripheral blood absolute blast count in patient 146 during dasatinib and avapritinib therapy.

Author Manuscript Author Manuscript Author Manuscript Author Manuscript

**Table 1:**

Genomic characteristics of patients with relapsed/refractory T-ALL enrolled on the LEAP Consortium trial (NCT02670525).

| # | Diagnosis | Mutations | Fusions | Cytogenetics/FISH |
|---|---|---|---|---|
| 7 | Refractory T-ALL | *JAK3, NOTCH1, WT1* | *AML1-LAF4* | 47,XX,t(2;21)(q11.1;q22),+der(7;21)(q10;q10),add(13)(q12)[6]/46,XX[14] |
| 19 | Refractory T-ALL | *TP53, WT1, CREBBP, JAK3* | *PICALM-MLLT10* | 46,XX |
| 56 | Refractory T-ALL | *PTEN* | *TRB-LMO1* | 46,XY |
| 79 | Relapsed T-ALL | *EZH2* | Not Assessed | 46,XX,t(7;14)(q32;q24)[18]/46,XX[2] |
| 89 | Relapsed T-ALL | *RUNX1, TP53, GNB1, PHF6* | None | 46,XY,−9,der(16)t(1;16)(p22;q24), +mar[cp14] |
| 127 | Relapsed T-ALL | *SETD2* | Not Assessed | 46,XY |
| 146 | Refractory T-ALL | *PDGFRA* | *STIL-TAL1, FIP1L1-PDGFRA* | 46,XX,del(9)(p13),del(13)(q14q32) [6]/46,sl, −1,−del(13),+mar[2]/46,XX[13] |
| 176 | Relapsed T-ALL | *NOTCH1, KRAS* | None | 45,XY,der(8;9)(q10;q10)[20] |
| 192 | Refractory T-ALL | *NOTCH1, NRAS, TP53, WT1* | *NUP214-ABL1* | 45,XY,der(6)t(6;17)(q27;q21),del(7)(p12p14),del(9)(p21.3),-17[13] |
| 230 | Refractory T-ALL | None | *STIL-TAL1, FIP1L1-PDGFRA* | 46,XY,del(6)(q15q23)[3]/46,XY[18] |
| 287 | Relapsed T-ALL | *WT1, NOTCH1, JAK3, PTPN11, IKZF1, JAK1, NFE2* | None | Karyotype failed |
| 293 | Relapsed T-ALL | *CREBBP, JAK1, JAK3, BCOR* | None | 46,XX,t(1;12)(p22;p11.2),t(2;6) (p21;p21)[14]/46,XX[6] |
| 298 | Relapsed T-ALL | None | None | 46,XX,del(9)(p21p24) |
| 329 | Relapsed T-ALL | *NOTCH1, STAT5B* | *STIL-TAL1* | 46,XY Loss in segment 9p21.3 with focal low level homozygous loss including CDKN2A/B genes |